INFLUENCE OF ELECTRIC PROPULSION ON PERFORMANCE AND FLIGHT MECHANICS OF VTOL AIRCRAFT

D. E. Lampl, S. F. Armanini
Technical University of Munich, TUM School of Engineering and Design,
Department of Aerospace and Geodesy, Lise-Meitner-Str. 9, 85521 Ottobrunn, Germany

Abstract

In recent years, electric vertical take-off and landing (eVTOL) aircraft have emerged as a promising alternative for urban air mobility (UAM). These aircraft, characterized by their wide altitude-velocity flight envelope, feature electric propulsion systems that are now part of the primary control system, introducing additional complexity in their design process. This study outlines a basic framework for the design, simulation, and analysis of eVTOL aircraft, with emphasis on understanding the impact of electric propulsion systems on flight mechanics and performance characteristics. The central part of our framework is a simulation of the flight dynamics using a multi-physics, multibody model based on the nonlinear equations of motion of a tiltrotor aircraft configuration. To show possible applications of the framework, we simulate a trimmed conversion flight, as well as the effect of a voltage drop at the tilting motors on an initially trimmed flight condition. The initial framework offers a flexible toolbox for eVTOL analysis, that can be easily adapted to different configurations. Future extensions of this framework will enable a more comprehensive investigation of the complex dynamics that govern eVTOL aircraft.

Keywords

Electric Propulsion; Flight Mechanics; Multibody Dynamics; Tiltrotor; VTOL Aircraft

1. INTRODUCTION

Thanks to recent advances in battery technology and power electronics, electric vertical take-off and landing (eVTOL) aircraft have the potential to provide a new and environmentally friendly mode of transportation, especially for urban air mobility (UAM) in densely populated regions [1–3]. These developments have led to a variety of innovative and unconventional eVTOL configurations in recent years. One of the main advantages of eVTOL aircraft is their wide altitude-velocity flight envelope compared to conventional airplanes or helicopters, which allows a wider range of missions [4]. They also feature different characteristics in terms of flight mechanics and performance. Moreover, performance (e.g. range) and flight dynamics aspects (e.g. stability and handling qualities) are connected via the electric propulsion system, which is now an integral part of the primary control system. Additionally, the aircraft can be fully controlled via differential thrust or tilting propellers, even without aerodynamic control surfaces. Consequently, the propulsion, energy storage and control system are coupled and thus also affect the overall flight performance. In summary, the interactions between aircraft subsystems increase the complexity of the overall aircraft system and its design process.
For example, the battery management system could limit the instantaneous power output after a peak power demand to avoid thermal runaway of the battery, which may reduce the maneuverability, flight performance and the boundaries of the flight envelope. As a result, the flight characteristics of certain flight modes cannot be investigated individually, as similar flight maneuvers may have different boundaries depending on the previous flight states. In addition, fast spinning and tilting propellers with relatively high masses and moments of inertia compared to the main airframe, may also impact the flight dynamics. Therefore, introducing these new aircraft require a profound understanding of their flight characteristics, especially in conjunction with the electric propulsion system.
Some studies have already investigated the flight mechanics of multibody eVTOL aircraft. However, these studies are often limited to specific flight conditions, such as hover and fixed-wing flight, or assume highly simplified configurations. In the following, we will give a short summary on some relevant studies.

doi: 10.25967/610120

A few non-electric VTOL aircraft like the experimental tiltrotor Bell XV-15 or the Osprey V-22 have been already intensively investigated in terms of flight mechanics [4,5]. However, those studies have not incorporated electric propulsion in their models. In Ref. [6], the equations of motion of a generic multibody tiltrotor aircraft are comprehensively derived using Kane's method. However, the authors did not explicitly include aerodynamic or electric motor models in their study. In a similar study, the authors of Ref. [7] also modeled a multibody tiltrotor aircraft but assumed that all nacelles could only be tilted synchronously. Reference [8] investigates the flight dynamics of a non-electric VTOL aircraft with two tilting propellers using Newton's laws. The authors of Refs. [9, 10] provide a comprehensive dynamic model including the multibody dynamics (MBD) and quasi-steady aerodynamics. The authors have not implemented an electric motor model, but used the rotor kinematics as control inputs, besides the conventional aerodynamic control surfaces. In Ref. [11], the author investigates flight mechanics and handling qualities of the pitch maneuver of a quadcopter configuration, including the electric motor dynamics. Other studies shift their focus on the aeroelastic effects using specialized software [12,13]. In summary, there is a clear need for detailed but generic multibody eVTOL model that includes the dynamics of the electric propulsion system.

Therefore, this study presents the basis for a preliminary framework for design, simulation, and analysis of eVTOL aircraft focusing particularly on the influence of the electric propulsion system on the flight mechanics and performance characteristics. For this, we develop a multibody, multi-physics simulation based on the nonlinear equations of motion of a representative aircraft, together with simplified aerodynamic and electric motor models. As a reference configuration we select a tiltrotor configuration sized for UAM with multiple fixed-pitched propellers and capable of fixed-wing cruise flight.

Since we expect that the rotor dynamics have a considerable effect on the overall dynamics, we model the aircraft as a multibody system using Kane's method. This also results in a generic and flexible framework that allows us to easily adapt the aircraft system, since each component is modelled independently [4]. Therefore, the approach can be easily extended to other configurations such as tilt-wing or lift+cruise with only minimal modification of the modeling structure. To verify our simulation setup and the implementation of the equations of motion, we model an electric tiltrotor aircraft with four engines and compare the simulation results to another study found in the literature. To give a brief perspective on possible applications, we also simulate a short open-loop conversion flight phase. In this simulation, we investigate the effect of a small drop in motor input voltage on an initially trimmed and steady longitudinal flight condition.

Following this introduction, Section 2 describes the aircraft model. The flight dynamics with the modeling of the kinematics, forces, and equations of motions are explained in Section 3. The section also describes the model implementation in Python and discusses the trimming of the eVTOL aircraft for longitudinal conversion flight. In Section 4, we present the simulation results, where we verify our implementation by comparing results to another study found in the literature. Then, we investigate the open-loop response of the aircraft to a small drop in motor input voltage. Finally, Section 5 summarizes the main conclusions and gives an outlook on future work.

2. AIRCRAFT MODEL

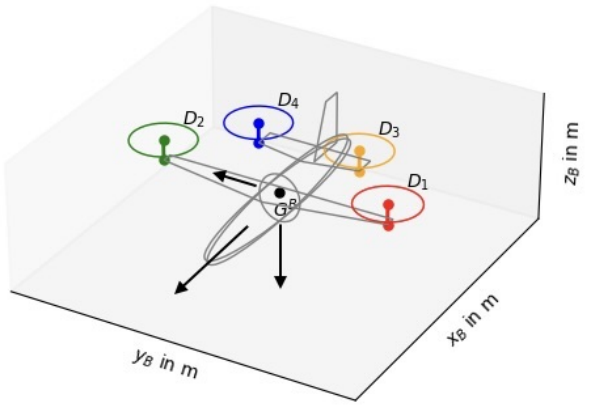

FIG 1. Tiltrotor aircraft model with four propellers.

In this study we consider a generic tiltrotor eVTOL aircraft with n_D propellers, each having a rotor disc mass of m_D and a moment of inertia of $\mathbf{I}_\mathrm{D}$ (with respect to the rotor-fixed reference frame). The basic aircraft model is based on Ref. [6]. Figure 1 sketches a tiltrotor aircraft model with four propellers. Aerodynamic control surfaces are not considered in this study.

The center of mass of each rotor disc $\mathrm{D_i}$ is denoted as G^{D_i}. The main rigid airframe B, which includes the fuselage, the fixed wings, and the tail, has mass m_B and moment of inertia $\mathbf{I}_\mathrm{B}$ (relative to its center of mass G^B and with respect to the body-fixed frame). The total mass of the aircraft model is therefore given by Eq. (1).

$$m = m_\mathrm{B} + m_\mathrm{D} n_\mathrm{D} \tag{1}$$

The airframe also defines the body-fixed reference frame B, which is located at the center of mass G^B of the airframe and oriented as shown in Fig. 1. Each individual rotor disc can rotate around itself, and is mounted on nacelles of length l_i, which can rotate

relative to the main airframe by a revolute joint, i.e. around the y_B axis. The nacelle masses are assumed to be zero but can be easily added to the model. The positions of the revolute joints P_i are fixed in frame B and are defined with respect to G^B. Consequently, the whole system has $n = (6 + 2n_\mathrm{D})$ degrees of freedom.

The position vector of the center of mass S of the entire aircraft system relative to G^B is given by Eq. (2), where $\vec{r}^{\,G^B G^{D_i}}$ is the position vector from G^B to G^{D_i}.

$$\vec{r}^{\,G^B S} = \frac{m_\mathrm{D}}{m} \sum_{i=1}^{n_\mathrm{D}} \vec{r}^{\,G^B G^{D_i}} \tag{2}$$

As inertial frame (N), we assume a flat and non-rotating earth. Besides that, the states are defined with respect to standard North-East-Down (O), body-fixed (B) and aerodynamic (A) reference frames. The inertial frame N has the same orientation as the frame O, but is fixed to the earth. Also, we use local reference frames fixed to the engine nacelle and rotor disc (D_i) for each propulsion system to define the corresponding forces and moments.

To describe the complete aircraft system, including the position relative to frame N, we need n generalized coordinates $\boldsymbol{q}$ and n generalized velocities $\boldsymbol{u}$, as defined in Eqs. (3) and (4). The generalized coordinates $\boldsymbol{q}$ are the minimum set of independent coordinates that can be used to describe the configuration of a system uniquely. Analogously, the generalized velocities $\boldsymbol{u}$ are the independent motion variables.

$$\boldsymbol{q} = [x, y, z, \Phi, \Theta, \Psi, \delta_1, \ldots, \delta_{n_\mathrm{D}}, \phi_1, \ldots, \phi_{n_\mathrm{D}}]^\mathsf{T} \tag{3}$$

$$\boldsymbol{u} = [u, v, w, p, q, r, \nu_1, \ldots, \nu_{n_\mathrm{D}}, \omega_1, \ldots, \omega_{n_\mathrm{D}}]^\mathsf{T} \tag{4}$$

Here, x, y and z describe the position of G^B in frame N. Φ, Θ and Ψ are the Euler angles between frame O and frame B. The angles δ_i and ϕ_i denote the nacelle tilt angle and the propeller angular position of the i-th rotor disc, respectively. The rotation matrix from frame B to frame D_i is given in Eq. (5).

$$\mathbf{M}_{D_i B} = \begin{bmatrix} 1 & 0 & 0 \\ 0 & \cos\phi_i & \sin\phi_i \\ 0 & -\sin\phi_i & \cos\phi_i \end{bmatrix} \cdot \begin{bmatrix} \cos\delta_i & 0 & -\sin\delta_i \\ 0 & 1 & 0 \\ \sin\delta_i & 0 & \cos\delta_i \end{bmatrix} \tag{5}$$

The velocity components of G^B in frame N, denoted in frame B, are depict as u, v and w. The angular velocities p, q, r are the roll, pitch and yaw rates, i.e. the angular velocity components of frame B with respect to frame O, denoted in frame B. The velocities ν_i and ω_i are the nacelle tilting angular velocity and the rotational speed of the rotor disc $\mathrm{D_i}$, respectively.

3. FLIGHT DYNAMICS

In this section, we present the flight dynamics of the generic VTOL aircraft discussed in Section 2. First, we derive the kinematic differential equations, before we describe the aerodynamic forces and moments acting on the aircraft. In a next step, we use Kane's method to derive the final equations of motion of this multibody system. Finally, we discuss the longitudinal trimming of the conversion mode.

3.1. Kinematics

The time derivative of the generalized coordinates $\dot{\boldsymbol{q}}$ and the generalized velocities $\boldsymbol{u}$ are linked via kinematic differential equations, i.e. $\dot{\boldsymbol{q}} = \boldsymbol{f}_\mathrm{k}(\boldsymbol{q}, \boldsymbol{u}, t)$. Together with the definitions $\nu_i = \dot{\delta}_i$ and $\omega_i = \dot{\phi}_i$, the attitude differential equations in Eq. (6) and the position differential equations in Eq. (7) (see next page) complete the set of n kinematic differential equations.

$$\begin{bmatrix} \dot{\Phi} \\ \dot{\Theta} \\ \dot{\Psi} \end{bmatrix} = \begin{bmatrix} 1 & \sin\Phi\tan\Theta & \cos\Phi\tan\Theta \\ 0 & \cos\Phi & -\sin\Phi \\ 0 & \sin\Phi/\cos\Theta & \cos\Phi/\cos\Theta \end{bmatrix} \cdot \begin{bmatrix} p \\ q \\ r \end{bmatrix} \tag{6}$$

3.2. Forces and Moments

In general, the gravitational force acting on a generic body J (with mass m_J and its mass center G^J) is independent of its attitude relative to other bodies and thus given by Eq. (8). Here, g is the gravitational acceleration.

$$\left(\vec{F}_G^{\,G^J}\right)_O = \begin{bmatrix} 0 \\ 0 \\ g\,m_J \end{bmatrix} \tag{8}$$

In the calculation of the aerodynamic forces we assume that no wind is present and that the aerodynamic lift, drag and side forces are only acting on the airframe with the wings. In Eq. (9), the aerodynamic forces are described with respect to the aerodynamic center A, and are denoted in the aerodynamic frame.

$$\left(\vec{F}_A^{\,A}\right)_A = q_\mathrm{dyn} S \begin{bmatrix} -C_D \\ C_Q \\ -C_L \end{bmatrix} \tag{9}$$

S is the wing reference area. C_Q, C_D and C_L are the side force, drag and lift coefficients, respectively. The latter two are defined below in Eqs. (10) and (11).

$$C_L = C_{L0} + C_{L\alpha}\alpha \tag{10}$$

$$C_D = C_{D0} + k_L C_L^2 \tag{11}$$

$$\begin{bmatrix}\dot{x}\\ \dot{y}\\ \dot{z}\end{bmatrix} = \begin{bmatrix}\cos\Psi\cos\Theta & \sin\Phi\sin\Theta\cos\Psi - \sin\Psi\cos\Phi & \sin\Phi\sin\Psi + \sin\Theta\cos\Phi\cos\Psi\\ \sin\Psi\cos\Theta & \sin\Phi\sin\Psi\sin\Theta + \cos\Phi\cos\Psi & -\sin\Phi\cos\Psi + \sin\Psi\sin\Theta\cos\Phi\\ -\sin\Theta & \sin\Phi\cos\Theta & \cos\Phi\cos\Theta\end{bmatrix} \cdot \begin{bmatrix}u\\ v\\ w\end{bmatrix} \tag{7}$$

Here, C_{D0} is the zero-lift drag coefficient, C_{L0} is the lift coefficient at zero angle of attack $\alpha = \arctan(w/u)$. $C_{L\alpha}$ depicts the lift curve slope, and k_L defines the lift-induced drag contribution.
The dynamic pressure q_{dyn} is calculated as defined in Eq. (12), where ρ is the air density. For simplification, we assume that the air density is constant with altitude.

$$q_{\mathrm{dyn}} = \frac{1}{2}\rho\left(u^2 + v^2 + w^2\right) \tag{12}$$

We can calculate the aerodynamic moments denoted in B frame around the aerodynamic center A with Eq. (13), where b is the wing span and c is the mean chord length.

$$\left(\vec{M}_A^{\,A}\right)_B = q_{\mathrm{dyn}} S \begin{bmatrix}C_l b/2\\ C_m c\\ C_n b/2\end{bmatrix} \tag{13}$$

C_l, C_m and C_n are the rolling, pitching and yawing moment coefficients.
For the rotor discs, we consider only the counteracting aerodynamic torques defined in Eq. (14) and denoted in the rotor disc frame D_i [4].

$$\left(\vec{M}_A^{\,G^{D_i}}\right)_{D_i} = -\operatorname{sgn}(\omega_i)\,\pi\rho R_i^5\omega_i^2 \begin{bmatrix}C_{\tau,i}\\ 0\\ 0\end{bmatrix} \tag{14}$$

R_i is the rotor disc radius and $C_{\tau,i}$ is the propeller torque coefficient. Since we can have counter-rotating rotors, we have to take the rotation direction into account, such that the aerodynamic torques are always acting against the rotation direction, assuming $C_{\tau,i} > 0$.
The rotor thrust force acting on a rotor disc is denoted in frame D_i and defined by Eq. (15), where $C_{T,i}$ describes the thrust constant [4]. Note that we assume that thrust is always positive.

$$\left(\vec{F}_P^{\,G^{D_i}}\right)_{D_i} = \pi\rho R_i^4\omega_i^2 \begin{bmatrix}C_{T,i}\\ 0\\ 0\end{bmatrix} \tag{15}$$

To control the aircraft, the aircraft has n_{D} electric motors, which create torques to tilt the nacelles as defined in Eq. (16), and n_{D} electric motors which power the propellers as shown in Eq. (17). These internal control torques shown here act on the rotor disc $\mathrm{D_i}$, but we also need to implement the reaction torques that act in opposite direction on the airframe B. The indices δ and ϕ denote the tilting and propeller motors, respectively.

$$\left(\vec{M}_\delta^{\,G^{D_i}}\right)_B = \begin{bmatrix}0\\ -K_{\nu,i}\,\nu_i + \frac{K_{\delta,V,i}}{R_{\delta,i}}V_{\delta,i}\\ 0\end{bmatrix} = -\left(\vec{M}_\delta^{\,G^B}\right)_B \tag{16}$$

$$\left(\vec{M}_\phi^{\,G^{D_i}}\right)_{D_i} = \begin{bmatrix}-K_{\omega,i}\,\omega_i + \frac{K_{\phi,V,i}}{R_{\phi,i}}V_{\phi,i}\\ 0\\ 0\end{bmatrix} = -\left(\vec{M}_\phi^{\,G^B}\right)_{D_i} \tag{17}$$

$K_{\nu,i}$ and $K_{\omega,i}$ are the motor damping constants for the tilting and propeller motors, which can include for example mechanical friction. $K_{\delta,V,i}$ and $K_{\phi,V,i}$ are the corresponding motor back-EMF constants. $R_{\delta,i}$ and $R_{\phi,i}$ represent the electrical resistance of the motors. The motors are controlled by the input voltages $V_{\delta,i}$ and $V_{\phi,i}$, which define the control input vector $\boldsymbol{c}$ of the aircraft system, as shown in Eq. (18).

$$\boldsymbol{c} = [V_{\delta,1},\ldots,V_{\delta,n_{\mathrm{D}}},V_{\delta,1},\ldots,V_{\phi,n_{\mathrm{D}}}]^{\mathsf{T}} \tag{18}$$

3.3. Equations of Motion

To derive the equations of motions for this aircraft, we use Kane's method. The following formulation shown here is based on Ref. [14].
Kane's method is a systematic approach to derive the equations of motion of a multibody system using generalized coordinates, velocities and forces, which can be easily solved numerically. Furthermore, using MBD ensures that the kinematics are exact, even if we approximate aerodynamic forces or structural dynamics, as all non-linear inertial terms are included [4]. In general, a multibody system is bounded by two types of constraints, which define how Kane's dynamical equations are derived: (holonomic) configuration constraints and (non-holonomic) motion constraints. In this study we have a holonomic system with no motion constraints. For a holonomic system, the number of degrees of freedom equals the number of generalized coordinates.

For a holonomic system with n degrees of freedom in the inertial frame N, the generalized active forces vector $\boldsymbol{F}_r = \boldsymbol{F}_r(\boldsymbol{q}, \boldsymbol{u}, t)$ and the generalized inertia forces vector $\boldsymbol{F}_r^\star = \boldsymbol{F}_r^\star(\boldsymbol{q}, \boldsymbol{u}, \dot{\boldsymbol{u}}, t)$ form the n Kane's dynamical differential equations in Eq. (19).

$$\boldsymbol{F}_r + \boldsymbol{F}_r^\star = \boldsymbol{0} \tag{19}$$

Since $\boldsymbol{F}_r^\star$ is linear in $\dot{\boldsymbol{u}}$ for a holonomic system, we can split the dynamical equations into the dynamic mass matrix $\mathbf{M}_d = \mathbf{M}(\boldsymbol{q}, t)$ and the dynamic forcing vector $\boldsymbol{f}_d = \boldsymbol{f}_d(\boldsymbol{q}, \boldsymbol{u}, t)$ using Eqs. (20) and (21), such that $\mathbf{M}_\mathrm{d}\dot{\boldsymbol{u}} = \boldsymbol{f}_d$.

$$\mathbf{M}_\mathrm{d} = -\mathbb{J}_{\boldsymbol{F}_r^\star}(\dot{\boldsymbol{u}}) \tag{20}$$

$$\boldsymbol{f}_\mathrm{d} = \boldsymbol{F}_r + \boldsymbol{F}_r^\star|_{\dot{\boldsymbol{u}}=\boldsymbol{0}} \tag{21}$$

$\mathbb{J}_{\boldsymbol{F}_r^\star}(\dot{\boldsymbol{u}})$ represents the Jacobian matrix of $\boldsymbol{F}_r^\star$ with respect to the time derivative of the generalized velocities $\dot{\boldsymbol{u}}$.
Finally, the complete equations of motion of a multibody system in reference frame N consist of the n kinematic differential equations and the n dynamical equations, hence in total $2n$ equations. Consequently, we can formulate the complete equations of motion in Eq. (22), where $\boldsymbol{x} = [\boldsymbol{q}, \boldsymbol{u}]^\mathsf{T}$ is the state vector of the whole system.

$$\mathbf{M}\,\dot{\boldsymbol{x}} = \begin{bmatrix} \mathbf{M}_k & \mathbf{0} \\ \mathbf{0} & \mathbf{M}_d \end{bmatrix} \begin{bmatrix} \dot{\boldsymbol{q}} \\ \dot{\boldsymbol{u}} \end{bmatrix} = \begin{bmatrix} \boldsymbol{f}_k \\ \boldsymbol{f}_d \end{bmatrix} = \boldsymbol{f} \tag{22}$$

Here, $\mathbf{M}_k$ is a $(n \times n)$ identity matrix, and $\boldsymbol{f}_k = \boldsymbol{f}_k(\boldsymbol{q}, \boldsymbol{u}, t)$ is the right-hand side of the kinematic differential equations. The complete derivation of the generalized forces is beyond the scope of this study and can for instance be found in Ref. [14].

3.4. Implementation

To implement our model we used Python, and specifically the symbolic Python library *SymPy*, a full-featured computer algebra system [15]. This library has the advantage that we do not need to manually derive the equations of motion, since Kane's method is already implemented in the library. Hence we can use the numerical methods available for the Python ecosystem to solve the coupled system without the need of a specialized software. For a given aircraft system, the SymPy function returns $\mathbf{M}$ and $\boldsymbol{f}$. The function requires the inertial reference frame N, the list of generalized coordinates $\boldsymbol{q}$ and velocities $\boldsymbol{u}$, as well as the kinematic differential equations from Section 3.1. To obtain the generalized active and inertia forces, we have to further define the bodies of the multibody system with their masses, moment of inertias, center of mass center and the reference frames in which the bodies are fixed. Furthermore, we need to provide the forces (with the point of application) and torques (with the reference frame) acting on the system.
To integrate the equations of motion over time t for a given set of initial conditions $\boldsymbol{x}_0 = \boldsymbol{x}|_{t=0}$, we can reformulate Eq. (22) to get an explicit form in Eq. (23).

$$\dot{\boldsymbol{x}} = \mathbf{M}^{-1}(\boldsymbol{x}, t)\boldsymbol{f}(\boldsymbol{x}, \boldsymbol{c}, t) \tag{23}$$

3.5. Trimmed Longitudinal Conversion Flight

In the process of trimming, we want to find the unknown control and state variables which define an equilibrium flight condition. This is usually done by solving a non-linear algebraic function [6]. In this study, we only consider longitudinal trimming. An analogous approach can be used to cover other flight conditions. Since eVTOL aircraft can not only transition between helicopter and airplane mode, but can also be trimmed and fully operated at a certain nacelle tilt angle, we call this part of the flight envelope *conversion mode* or *conversion flight* [4]. We define trimmed longitudinal conversion flight as a steady, level flight at a desired horizontal velocity $\dot{x}_\mathrm{trim}$, i.e. $\dot{x} = \dot{x}_\mathrm{trim}$ and $\dot{z} = 0$, and set all tilt angles to $\delta_i = \delta_\mathrm{trim}$. Both the airplane and helicopter mode, e.g. hover flight, are special cases of the conversion flight, where all tilt angles are zero or $\delta_\mathrm{trim} = 90°$, respectively. We solve for the unknown $(3 + 4n_\mathrm{D})$ trim variables $\boldsymbol{x}_s$ in Eq. (24), which consist of the control voltage inputs and the unknown states.

$$\boldsymbol{x}_s = \left[\Theta, u, w, \omega_1, \ldots, \omega_{n_\mathrm{D}}, \dot{\phi}_1, \ldots, \dot{\phi}_{n_\mathrm{D}}, \boldsymbol{c}\right]^\mathsf{T} \tag{24}$$

For longitudinal trimming, all other states $\boldsymbol{x} = \boldsymbol{x}_\mathrm{trim}$ and time derivatives $\dot{\boldsymbol{x}} = \dot{\boldsymbol{x}}_\mathrm{trim}$ are set to zero. This includes the x, y, z, ϕ_i and Ψ states, which have no influence on the trim solution. To minimize the residuals $\boldsymbol{g}(\boldsymbol{x}_s)$ in Eq. (25), we define a least-squares problem as shown in Eq. (26).

$$\boldsymbol{g}(\boldsymbol{x}_s) = [g_1, \ldots, g_n]^\mathsf{T} = \mathbf{M}^{-1}(\boldsymbol{x}_s)\boldsymbol{f}(\boldsymbol{x}_s) - \dot{\boldsymbol{x}}_\mathrm{trim} \tag{25}$$

$$\min_{\boldsymbol{x}_s} \|\boldsymbol{g}(\boldsymbol{x}_s)\|_2^2 \tag{26}$$

We also defined appropriate lower and upper bounds for the trim variables, which are considered in the optimization as constraints.

4. RESULTS AND DISCUSSION

In this section, we provide an initial demonstration of our simulation framework's capabilities for analyzing the effects of electric propulsion on the flight mechanics of eVTOL aircraft. Note that the simulations should be considered as academic case studies and do not

accurately replicate real-life flight conditions, since the selected parameters do not necessarily correspond to a real aircraft. Although the complete equations of motion are implemented, in the following simulations we consider only the longitudinal motion of a tiltrotor aircraft with four rotors.
First, to verify our implementation, we simulate the response of the aircraft to given initial conditions and compare our results to results from the literature.
In a second simulation, we trim the aircraft to conversion flight and simulate a drop of the input voltages at the tilt motors. The voltage drop is a simplified example of a potential failure mode, however it may not be representative for a real flight situation, especially, as we have not yet incorporated a flight control system.

4.1. Simulation Setup

We used the same aircraft properties as defined in [6]. The relative position of the tilt joints and the propellers is also shown to scale in Fig. 1.

- Masses:
  $m_\mathrm{B} = 2176.0\,\mathrm{kg}$, $m_\mathrm{D} = 118.0\,\mathrm{kg}$
- Nacelle lengths:
  $l = 1.0\,\mathrm{m}$
- Moments of inertia:

$$\left(\mathbf{I}^{G^B}\right)_{BB} = \begin{bmatrix} 74110 & 0 & 0 \\ 0 & 6780 & 0 \\ 0 & 0 & 74529 \end{bmatrix} \mathrm{kg\,m^2}$$

$$\left(\mathbf{I}^{G^{D_i}}\right)_{D_iD_i} = \begin{bmatrix} 137 & 0 & 0 \\ 0 & 69 & 0 \\ 0 & 0 & 69 \end{bmatrix} \mathrm{kg\,m^2}$$

- Tilt joint position:
  $(\vec{r}^{\,G^BP_1})_B = [0.5, -5.5, -0.25]^\mathsf{T}\,\mathrm{m}$,
  $(\vec{r}^{\,G^BP_2})_B = [0.5, 5.5, -0.25]^\mathsf{T}\,\mathrm{m}$,
  $(\vec{r}^{\,G^BP_3})_B = [-2.5, -2.5, -0.5]^\mathsf{T}\,\mathrm{m}$,
  $(\vec{r}^{\,G^BP_4})_B = [-2.5, 2.5, -0.5]^\mathsf{T}\,\mathrm{m}$

4.2. System Response

In this simulation example, we verify our model by comparing the simulation results to the results from [6]. Here, we simulate the response of the multibody system to given inital conditions. To allow for a direct comparison to Ref. [6], all internal and external forces, such as gravity or thrust, are neglected. The initial values are visible in Fig. 2 at $t = 0\,\mathrm{s}$. At the beginning, we also set $\delta_i = 0°$ for all engine nacelles, which corresponds to the airplane mode.
The comparsion of the results in Fig. 2 shows that the simulation results are similar, but not identical. Note that the markers in the plots are just used to differentiate curves and thus do not represent all values. Because the implementation of the equations of motion is the same in the absence of any forces and torques, we suppose that any variations from Ref. [6] are due to numerical and integration errors, since the differences increase as the simulation progresses. For example, in contrast to the simulation from [6], where δ_1 becomes positive after a few seconds, in our simulation we have $\delta_3 > 0$ and $\delta_1 < 0$ at approximately the same time step (not shown).
Nonetheless, the close agreement of the velocities with the reference, as well as the initial agreement of the angular rates, suggest a correct implementation of the equations of motion.

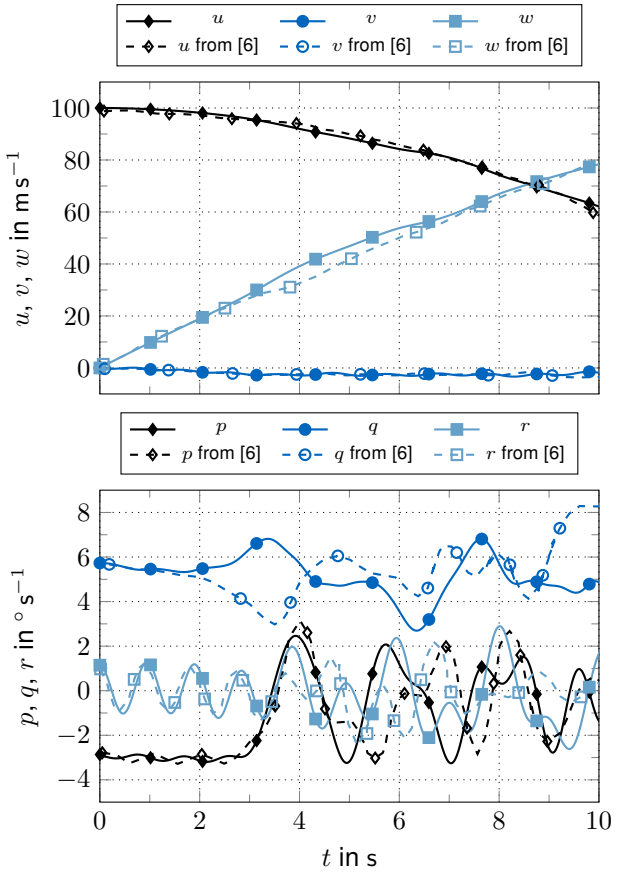

FIG 2. Comparison of the system response to the simulation results from Ref. [6].

4.3. Conversion Flight

For the conversion flight simulation with all external forces and moments, we set the initial desired horizontal velocity to $\dot{x} = \dot{x}_\mathrm{trim} = 50\,\mathrm{m\,s^{-1}}$ and the initial collective tilt angle to $\delta_i = \delta_\mathrm{trim} = 80°$. The other parameters are defined as follows:

- General:
  $g = 9.81\,\mathrm{m\,s^{-2}}$, $\rho = 1.225\,\mathrm{kg\,m^{-3}}$, $S = 15.0\,\mathrm{m^2}$
- Aerodynamics:
  $(\vec{r}^{\,G^BA})_B = [-0.5, 0, 0]^\mathsf{T}\,\mathrm{m}$ (position of point A),
  $C_{L0} = 0.3$, $k_L = 0.04$, $C_{L\alpha} = 0.9 \cdot 2\pi\,\mathrm{rad^{-1}}$,
  $C_{D0} = 0.05$, $C_Q = 0$, $C_l = C_m = C_n = 0$
- Propellers:
  $R_i = 1.5\,\mathrm{m}$, $C_{T,i} = 0.05$, $C_{\tau,i} = 0.01$

- Electric Motors:
  $K_{\nu,i} = K_{\omega,i} = 10\,\mathrm{N\,m\,s\,rad^{-1}}$,
  $K_{\delta,V,i} = K_{\phi,V,i} = 0.4\,\mathrm{N\,m\,A^{-1}}$, $R_{\delta,i} = R_{\phi,i} = 0.1\,\Omega$

4.3.1. Trimmed Conditions

Before trimming, we set upper and lower bounds for the states and inputs to get a trim solution with counter-rotating propellers at the wings and tail, e.g. $\omega_1 > 0$ and $\omega_2 < 0$, and to avoid the singularity at $\cos\Theta = 0$. The trimmed solution is then used as initial condition for the simulation. Figure 3 sketches the aircraft in trimmed conversion flight. We get the following values for the trimmed states:

- Attitude:
  $\Theta = 3.06° = \alpha$
- Velocity:
  $u = 49.93\,\mathrm{m\,s^{-1}}$, $w = 2.67\,\mathrm{m\,s^{-1}}$
- Propeller Velocity:
  $\omega_1 = -\omega_2 = 76.30\,\mathrm{rad\,s^{-1}}$, $\omega_3 = -\omega_4 = 21.57\,\mathrm{rad\,s^{-1}}$
- Motor Voltage:
  $V_{\delta,i} = 34.99\,\mathrm{V}$,
  $V_{\phi,1} = -V_{\phi,2} = 616.09\,\mathrm{V}$, $V_{\phi,3} = -V_{\phi,4} = 87.92\,\mathrm{V}$

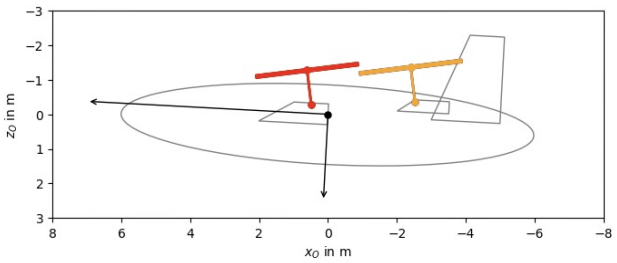

FIG 3. Aircraft in trimmed conversion flight.

Figures 4 and 5 show, that the aircraft is able to maintain the trimmed state in the first $5\,\mathrm{s}$, prior to any actuation. Here, the lift-to-weight ratio is $L/(mg) = 0.532$, the total thrust amounts $12.249\,\mathrm{kN}$. The steady center of mass position of the aircraft system is found to be $(\vec{r}^{\,G^B S}_{\mathrm{trim}})_B = [-0.147, 0, -0.242]^\mathsf{T}\,\mathrm{m}$.

4.3.2. Response to Voltage Drop

We run the simulation for $15\,\mathrm{s}$. For the first $5\,\mathrm{s}$, we fly in the trimmed conversion flight mode. At $t = 5\,\mathrm{s}$, we gradually reduce the applied motor voltages $V_{\delta,i}$ of the tilt motors to $75\,\%$ of the trimmed voltage at $t = 5.5\,\mathrm{s}$, where we increase the voltages again to the previously voltage level, as shown at the top in Fig. 4. Since the voltage decreases, the nacelle should tilt forward, as we have less motor torque counteracting the moment due to the gravitational force acting on the rotor discs.
After the voltage drop, we indeed see in Fig. 4 that all rotors tilt forward. However, the aircraft cannot recover from this voltage drop by itself without a flight controller. At about $t = 8\,\mathrm{s}$, the aircraft starts to become unstable and and loses altitude. The propeller speeds ω_i do not change, since we have no lateral motion, i.e. $p = r = \dot{p} = \dot{r} = 0$, and the applied torques are constant.
While this is just a simplified example without a flight controller, it demonstrates that we need to incorporate MBD and the electric system dynamics in order to understand the flight characteristics of eVTOL aircraft.

5. CONCLUSION

We developed the basis of a preliminary design and analysis framework for eVTOL aircraft. The focus is on investigating the influence of electric propulsion on flight mechanics characteristics. At the center of our framework is a dynamic simulation model. We implemented the corresponding equations of motion for a generic multibody tiltrotor aircraft in Python using Kane's method, including simplified aerodynamic and electric motor models.
The framework can be used to evaluate how and to what extend flight mechanic properties and performance metrics of eVTOL are coupled. As we showed in the simulation result, the framework allows also to trim the aircraft in longitudinal conversion flight mode, i.e. forward flight with tilted rotors. Hence, we can determine how the boundaries of the conversion flight envelope scale with different parameters. On the other hand, possible implications on the design of the electric system could be drawn, such as sizing the system not only for the overall mission but also for certain flight maneuvers. In addition, the simulation program can help in the development of new flight control architectures for eVTOL aircraft. The framework can be easily extended to other aircraft configurations, or modified to include more sophisticated electric system and aerodynamic models.
In a next step, we will model the dynamics of the whole electric system architecture, including the battery system. For further analysis, including other flight modes such as fixed-wing flight, a suitable flight control system needs to be developed. Also, although we have verified our model by comparing our simulation results to a similar study in the literature, validation with experimental data would be valuable.
In summary, the results of the study show that the framework is able to analyze and simulate the flight mechanics of a generic multibody tiltrotor aircraft. The presented approach provides a simple but generic tool for preliminary investigations of the flight mechanics and performance of eVTOL aircraft.

Contact address:

david.lampl@tum.de

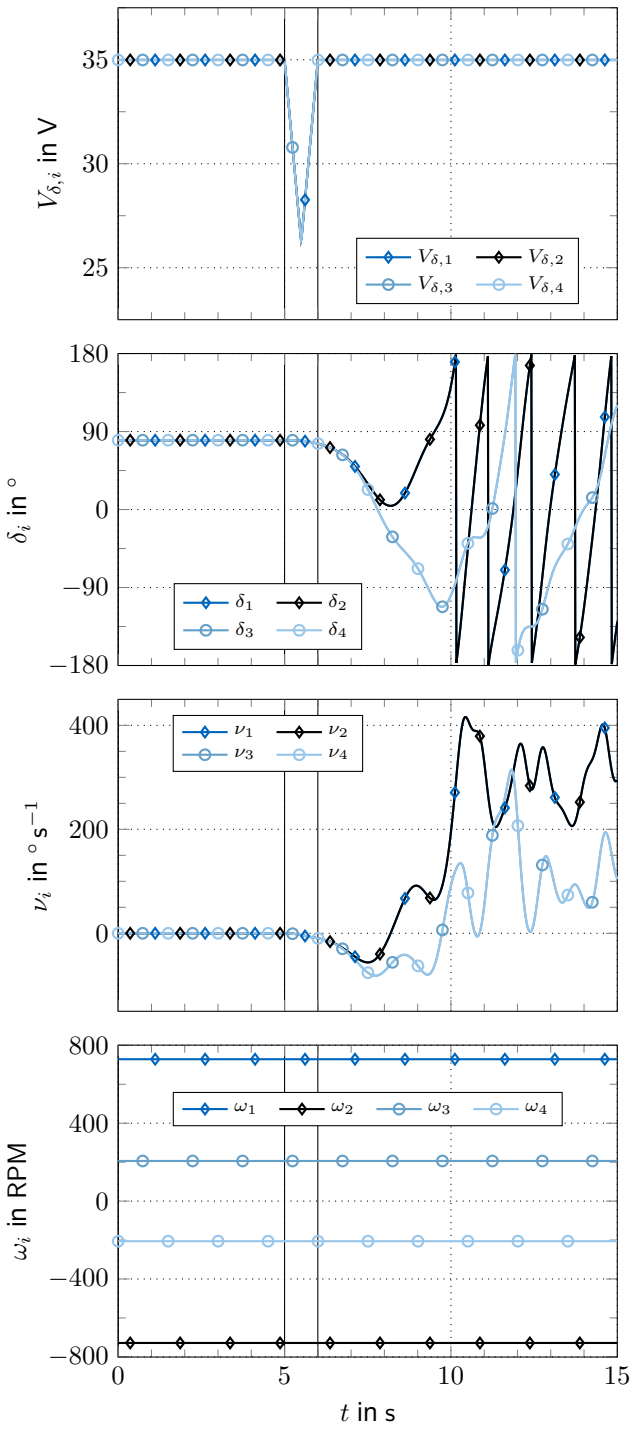

FIG 4. Input voltages for the tilting motors $V_{\delta,i}$, nacelle tilt angles δ_i, tilting angular rates ν_i, and propeller speeds ω_i during the conversion flight.

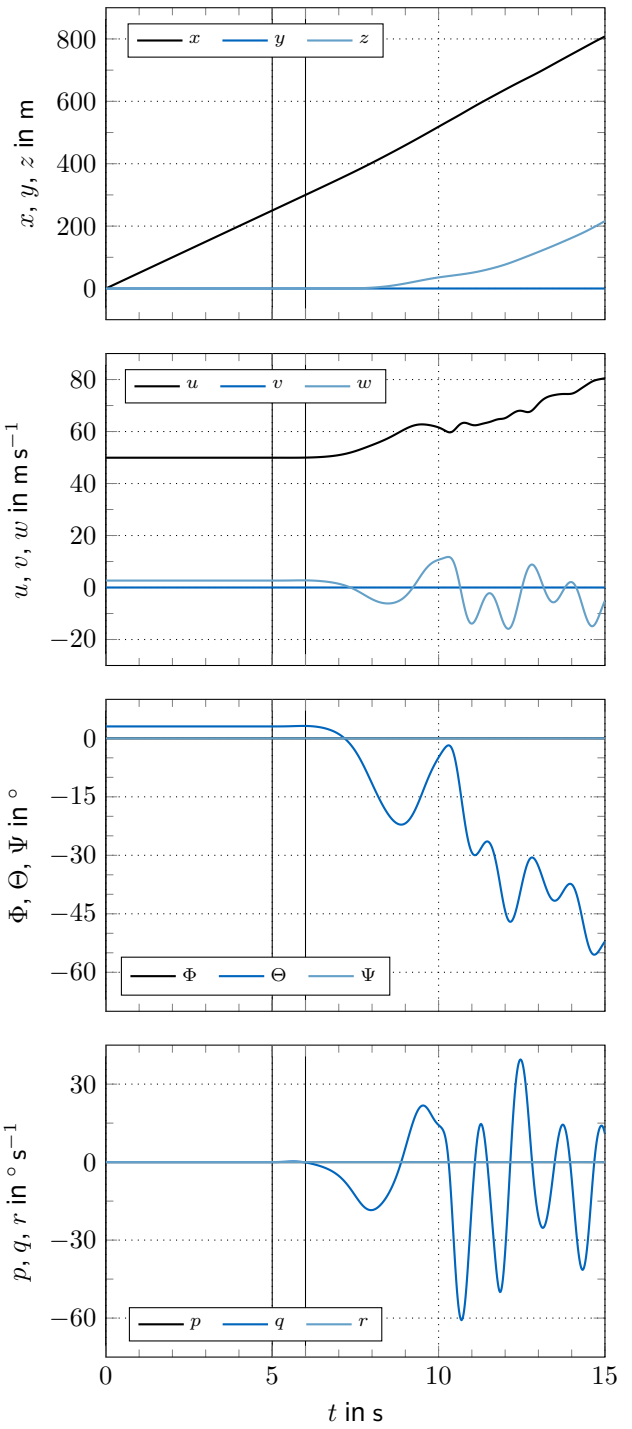

FIG 5. Position (x, y, z), velocity (u, v, w), attitude (Φ, Θ, Ψ), and angular velocity (p, q, r) during the conversion flight.

References

[1] S. Rajendran and S. Srinivas. Air taxi service for urban mobility: A critical review of recent developments, future challenges, and opportunities. *Transportation Research Part E: Logistics and Transportation Review*, 143:102090, 2020. DOI: 10.1016/j.tre.2020.102090.

[2] A. Bauranov and J. Rakas. Designing airspace for urban air mobility: A review of concepts and approaches. *Progress in Aerospace Sciences*, 125:100726, 2021. DOI: 10.1016/j.paerosci.2021.100726.

[3] C. Al Haddad, E. Chaniotakis, A. Straubinger, K. Plötner, and C. Antoniou. Factors affecting the adoption and use of urban air mobility. *Transportation Research Part A: Policy and Practice*, 132:696–712, 2020. DOI: 10.1016/j.tra.2019.12.020.

[4] G. D. Padfield, editor. *Helicopter Flight Dynamics: Including a Treatment of Tiltrotor Aircraft*. Wiley, 1 edition, 2018.

[5] G. L. Ghiringhelli, P. Masarati, P. Mantegazza, and M. W. Nixon. Multi-Body Analysis of a Tiltrotor Configuration. *Nonlinear Dynamics*, 19(4):333–357, 1999. DOI: 10.1023/A:1008386219934.

[6] J. Pei and C. Roithmayr. Equations of Motion for a Generic Multibody Tilt-rotor Aircraft. In *AIAA AVIATION 2022 Forum*, Chicago, IL & Virtual. American Institute of Aeronautics and Astronautics. DOI: 10.2514/6.2022-3511.

[7] J. Su, C. Su, S. Xu, and X. Yang. A Multibody Model of Tilt-Rotor Aircraft Based on Kane's Method. *International Journal of Aerospace Engineering*, 2019, 2019. DOI: 10.1155/2019/9396352.

[8] L. Haixu, Q. Xiangju, and W. Weijun. Multibody Motion Modeling and Simulation for Tilt Rotor Aircraft. *Chinese Journal of Aeronautics*, 23(4):415–422, 2010. DOI: 10.1016/S1000-9361(09)60236-3.

[9] W. Su, S. Qu, G. Zhu, S. S.-M. Swei, M. Hashimoto, and T. Zeng. Modeling and control of a class of urban air mobility tiltrotor aircraft. *Aerospace Science and Technology*, 124:107561, 2022. DOI: 10.1016/j.ast.2022.107561.

[10] W. Su, S. Qu, G. G. Zhu, S. S.-M. Swei, M. Hashimoto, and T. Zeng. A Control-Oriented Dynamic Model of Tiltrotor Aircraft for Urban Air Mobility. In *AIAA Scitech 2021 Forum*. American Institute of Aeronautics and Astronautics, 2021. DOI: 10.2514/6.2021-0091.

[11] M. D. Pavel. Understanding the control characteristics of electric vertical take-off and landing (eVTOL) aircraft for urban air mobility. *Aerospace Science and Technology*, 125:107143, 2022. DOI: 10.1016/j.ast.2021.107143.

[12] A. Savino, A. Cocco, A. Zanotti, M. Tugnoli, P. Masarati, and V. Muscarello. Coupling Mid-Fidelity Aerodynamics and Multibody Dynamics for the Aeroelastic Analysis of Rotary-Wing Vehicles. *Energies*, 14(21):6979, 2021. DOI: 10.3390/en14216979.

[13] M. Mattaboni, P. Masarati, G. Quaranta, and P. Mantegazza. Multibody Simulation of Integrated Tiltrotor Flight Mechanics, Aeroelasticity and Control. *Journal of Guidance, Control, and Dynamics*, 35(5):1391–1405, 2012. DOI: 10.2514/1.57309.

[14] C. M. Roithmayr and D. H. Hodges. *Dynamics: Theory and Application of Kane's Method*. Cambridge University Press, 2016.

[15] SymPy, 2023. https://www.sympy.org/en/index.html.